

CHAPTER 4

Viscometers

AGÍLIO A. H. PÁDUA, DAISUKE TOMIDA, CHIAKI YOKOYAMA,
EVAN H. ABRAMSON, ROBERT F. BERG, ERIC F. MAY,
MICHAEL R. MOLDOVER AND ARNO LAESECKE

4.1 Vibrating-wire Viscometer

AGÍLIO A. H. PÁDUA

Vibrating-wire sensors have been prominent in viscometry ever since the measurements in liquid He in the 1960s¹ using the attenuation of transverse oscillations in a tensioned wire; the measurement was founded on a hydrodynamic analysis by Stokes of the damping of fluids on oscillating bodies. Our understanding of the technique has since progressed considerably, driven by W.A. Wakeham and collaborators who designed viscometers for wide ranges of conditions. Vibrating-wire viscometers² and densimeters³ were reviewed in previous books in this series. The field has seen significant developments over the last twenty years and is active at present, with improvements and extensions of the capabilities of the method.

Curiously, two communities work on vibrating-wire viscometers: one of low-temperature physicists studying superfluid ⁴He and ³He at temperatures below 1 mK. Recent reports in this field use vibrating-wire probes to observe hydrodynamic phenomena in quantum liquids⁴ and not primarily to determine viscosity accurately. The other community, of physical chemists and chemical engineers, studies transport properties for application in devices and processes, often at high pressure (up to 1 GPa),⁵ seeking to improve the quantitative determination of viscosity. About 200 scientific papers deal with

vibrating-wire measurements, so a full account on the field is not possible here. The main recent developments concern:

1. Performing absolute viscosity measurements.
2. Extending the operation limits towards gases or high-viscosity liquids.
3. Characterising new viscosity reference substances.
4. Improving our understanding of the sensor (mode of operation, detection or simultaneous density measurements).
5. Designing robust and practical sensors for measurements *in situ*.

4.1.1 Principle of Operation

In a vibrating-wire viscometer the damping of transverse oscillations is related to the viscosity of the surrounding fluid. This setup benefits from a complete and accurate physical description. First, the mechanics of oscillation of a thin rod is described within the elastic limit for clamped, pinned or free end conditions. Second, the hydrodynamics associated with the motion of the wire in an incompressible, Newtonian fluid is understood.^{6,7} Third, the output signal is resolved using equivalent circuits,⁸ although optical detection has been reported.⁹ The three pieces of the analytical model are rigorous within defined limits^{6,7} that can be met in practice. The working equations are slightly different for steady-state or decay modes, and the equivalent circuit depends on the instrumentation, so the reader is referred to the literature.^{6-8,10,11} The main point is that the sensor response is expressed purely in terms of physical parameters of the wire (length, radius, density, Young's modulus), and of the density and viscosity of the fluid. The theory specifies conditions: the radius of the wire must be much smaller than its length and the amplitude of vibration small, the walls of the container must be distant from the wire, the compressibility of the fluid negligible, and the flow laminar. A vibrating-wire viscometer should be able to perform absolute measurements (without calibration against a standard) provided its parameters are characterised by independent means and the fluid density is known.

The vibrating-wire viscometer is composed of a conducting wire tensioned in a support, placed inside a permanent magnetic field, both to drive the sensor and to obtain its response. The magnets can be mounted outside the enclosure or high-pressure vessel,¹²⁻¹⁴ for a smaller volume, higher pressure range, and no compatibility issues between the magnets and the sample. The drawbacks are that the vessel has to be non-magnetic (which can limit the pressure) and the magnets bigger. In other designs the magnets, sometimes gold-plated to improve corrosion resistance, are inside the pressure vessel^{11,15} forming a tightly integrated sensor suitable for *in situ* measurements.¹⁶ It is often reported that the magnetic field should be aligned with certain directions imposed by the wire or the mounting in order to select a pure resonance, otherwise two resonant frequencies are observed, due to anisotropy of the wire material, an elliptical cross-section or to deformations produced by the clamping fixture.

The wire is driven into transverse oscillations by an alternating current, which generates a periodic force, and the velocity is detected as a voltage induced by the displacement in the magnetic field.^{8,17} This electro-mechanical oscillator interacts with other electrical impedances of the instrumentation, which must be accounted for in order to extract the intrinsic signal of the sensor.^{8,18–20} Some non-viscous damping is present, either due to inelastic loss within the wire (negligible at low amplitudes), friction at the clamped ends or magnetic damping.^{8,17,21} Non-viscous damping is independent of the fluid and is evaluated by a measurement of the resonant characteristics in vacuum.^{6,7} Non-viscous damping becomes more relevant for low viscosities (gases).²¹

The sensor can be operated in either forced, steady-state or in ring-down, transient decay. The decay mode was initially the choice for viscometry.^{1,22,23} The wire is set into forced vibration or plucked for a few cycles and then the free damped oscillations are recorded, as shown in Figure 4.1. The typical time for one acquisition is 20 ms in liquids^{23,24} and 100 ms in gases,²¹ so multiple sampling can be done to reduce noise. Because of the short time, the transient mode is suitable for online, flow measurements.²⁴ The working theory limits the lateral displacement to a few per cent of the wire radius. In the transient mode, however, the wire is driven at relatively high amplitudes,²⁵ and, especially for gases where thinner wires are used, it is important to check the applicability of the theory by extrapolating to zero amplitude.²¹

In the forced mode a frequency range encompassing the resonance peak is scanned to describe amplitude and phase,^{12,20} as shown in Figure 4.2.

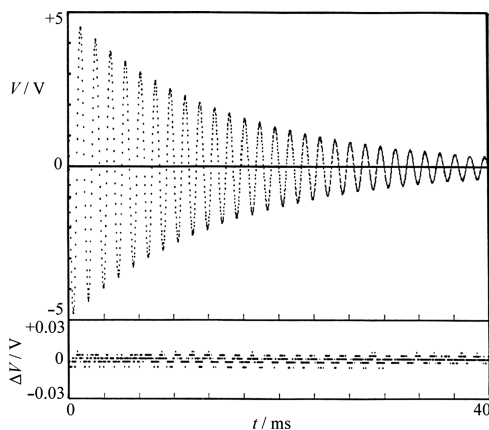


Figure 4.1 Top: Output motional electric potential difference V of the vibrating-wire viscometer immersed in methylbenzene operated in the transient mode as a function of time t .²⁶ Bottom: ΔV difference between the measured electric potential difference and that obtained from the working equations with the optimized viscosity at a known density.

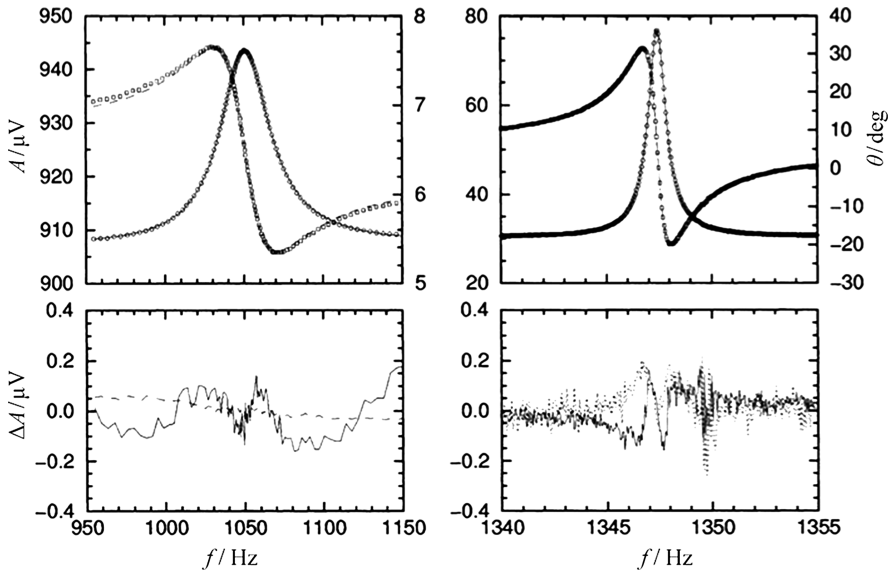


Figure 4.2 Output amplitude A and phase θ of the vibrating viscometer operated in forced oscillation. Left: vibrating wire immersed in water. Right: vibrating wire immersed in vacuum.¹² In this case, the wire was clamped at the upper end in a rigid support. A mass was suspended from the lower end so that, invoking Archimedes principle, the density was also determined simultaneously from the variation of the resonance frequency. The lines are those obtained from the working equations.

A lock-in amplifier filters out noise outside the frequency of interest and is extremely sensitive, allowing the wire to be driven at low amplitudes. The acquisition of one curve can take 600 s because the signal must stabilize after each frequency step. To have the best of both worlds, researchers devised ways of accounting for the nonlinear effects at high amplitudes²⁵ and use the transient mode for fast and accurate measurements.

One issue in viscometry is that the density of the fluid must be known to determine the dynamic viscosity, since the hydrodynamics of the measurement involve viscous and inertial terms. The vibrating wire is sensitive to the density through an added, hydrodynamic mass of fluid accelerated with the wire. Unfortunately, the sensitivity arising from the hydrodynamic mass is not sufficient for a precise determination of density. To circumvent this, a vibrating-wire viscometer can be coupled with a densimeter²⁷ and both properties measured simultaneously. An elegant alternative is to amplify the sensitivity to the density using Archimedes' principle.^{10,12,18,28} In this design the vibrating wire is vertically tensioned by a suspended weight that will define the resonant frequency in vacuum. When the wire and weight are immersed in a fluid, the buoyancy on the weight lowers the resonant frequency (Figure 4.2). The measurement of density and viscosity is an enormous advantage but has some downsides. First, the instrument is delicate

because of the suspended weight. Also, the “return” of the signal requires a connection on the weight without altering the wire tension. Last, the volume of the weight must be known. But the vibrating-wire densimeter–viscometer is also described by rigorous theory. It was used at pressures up to 200 MPa providing relative uncertainties ($k = 2$) in density and viscosity of $\pm 0.2\%$ and $\pm 2\%$, respectively.^{10,12,18,28}

4.1.2 Absolute *versus* Relative Measurements

The distinction between absolute and relative measurements is not binary. A relative method is one without a full theory and the working equations contain empirical parameters whose values are determined using reference substances, often in the same conditions as the measurements, and even with properties similar to the sample. An absolute method is described by accurate equations containing only quantities with rigorous physical sense, accessible independently. Such a method will produce accurate results in diverse conditions. But, because of practical limitations, it may happen that a rigorous theory is available but some of the physical parameters are difficult to determine independently with the required accuracy. That method will be quasi-absolute in the sense that calibration is necessary to obtain the one or few problematic parameters, and this can be done using standard samples and conditions. From then, the accuracy should match that of a truly absolute method. The calibration step may hide deficiencies and some parameters will be “effective”, compensating or averaging aspects that are not described well, lowering uncertainty far from the calibration point. This discussion is pertinent for measurements in general, but for viscosity it is crucial because few substances qualify as standards, and viscosity can cover many orders of magnitude according to chemical composition, temperature or pressure. Such an extent places a demanding requirement on viscometry techniques, thence the search for absolute methods.

It was demonstrated that the vibrating-wire viscometer is absolute, provided special care is taken in the manufacture and characterization of its components. The radius of the wire is the most difficult parameter to determine independently (radii range from 10 μm for gases, to 50 μm for liquids, and up to 200 μm for high viscosities). The uniformity and shape of the cross-section are important issues, as is the surface smoothness. Tungsten is chosen because of its high density, Young’s modulus and tensile strength, low thermal expansion and chemical inertness. Until recently most viscometers had been built with wire of high purity but poorly characterised radius, therefore they were operated in a quasi-absolute manner, determining the radius from one calibration point. To measure the density simultaneously using the buoyancy effect, the volume of the weight should be known within $\pm 0.1\%$. This volume can be obtained together with the wire radius from one calibration (in water¹² or methylbenzene¹⁸) although it can be determined independently.¹⁰ For operation in wide ranges of conditions it is important to take into account the effects of temperature

and pressure on the wire (and weight), so it is better to select materials with well-known thermal expansion coefficients and compressibility (and the temperature-dependence of Young's modulus¹⁰).

Only recently, two groups^{10,29} tested sensors built with carefully prepared tungsten wires, obtained through grinding to a uniform section. In one report²⁹ the radius of the wire was measured independently in a metrology laboratory with a relative uncertainty of 3×10^{-4} . Electron microscopy showed much smoother surfaces than those of simply drawn wires.¹⁰ "Calibration" of the radii of the ground wires using reference fluids yielded values that coincided with the independent measurements.¹⁰ Absolute measurements²⁹ of the viscosity of water at $T = 293.15$ K and $p = 101.325$ kPa yielded $(1.001_9 \pm 0.009_0)$ mPa · s, differing from the standard value relatively by 0.03 %. The sensitivity of the vibrating-wire viscometer can still be improved by using a thinner wire. Therefore, it was demonstrated that the vibrating-wire viscometer is absolute provided all its physical parameters are characterised.

4.1.3 High-viscosity Standards

Viscosity has enormous scientific and industrial importance, and many applications concern samples of significantly higher viscosity than water, as has been discussed in section 2.2.5. Since most viscometers are relative, with limited ranges, calibration at high viscosities involves several transfers to ensure traceability to the standard substance, a costly procedure subject to error propagation. No reference substance exists at high pressure, a limitation affecting domains from lubricants to reservoir fluids. Several hydrocarbons have been recommended as high-pressure references (up to 250 MPa for toluene³⁰) but these are low-viscosity liquids. Vibrating-wire viscometers are suited to produce high-pressure data because they are composed of solid bodies and the working model is rigorous. They were used to characterise candidates for high-viscosity standards³¹ such as 2,6,10,15,19,23-hexamethyltetracosane (commonly known as squalane)³² and diisodecyl phthalate (DIDP)^{11,14,33} at pressures above 100 MPa, with viscosities reaching 267 mPa · s.³⁴ Various laboratories used different methods for comparison and some deviations arise from variations in sample purity.^{35,36} Recent reports^{11,14} review the data showing relative uncertainties of ± 2 % for vibrating-wire measurements and agreement between different techniques within ± 5 % (except for certain discrepancies^{31,33}).

In the range above 100 mPa · s, damping is high and vibrating-wire sensors are operated at low quality factors,³³ which is not a problem to the hydrodynamic model, but the amplitude becomes difficult to detect (either attenuation is too rapid or the resonance peak is too flat). So the limit for high-viscosity samples is resolution. Recommended thermophysical property data should always be obtained using different techniques to avoid systematic errors and this provides an important role for the vibrating-wire method.

4.1.4 Expanding the Limits: Complex Fluids and Online Measurements

Recently several attempts expanded the limits of vibrating-wire viscometry, towards complex fluids and towards robust and practical sensor designs. Vibrating-wire viscometers were used with industrially-relevant fluids, such as non-chlorinated refrigerants³⁷ or bio-sourced components of fuels.³⁸ Low uncertainty measurements are never simple, but today the vibrating-wire method is well understood in organic liquids. Asymmetric mixtures, of molecules with different sizes or interactions, are challenging because variations in composition lead to large viscosity changes. Vibrating-wire viscometer–densimeters have been used with gas-condensate mixtures³⁹ and lubricant/refrigerant mixtures.^{32,40} The overall uncertainties are comparable to those in pure liquids, demonstrating that vibrating-wire sensors can be used to study complex samples.

Electrically-conducting fluids have been approached with more suspicion. Even water was used as a calibrant only in 2001¹² (after one isolated report⁴¹) because of eventual corrosion or conduction, but today is the reference fluid of choice.^{10,29} Ionic liquids demonstrate the applicability of the method to conducting fluids.^{20,42} The conductivity of these salts is not enough to shunt the sensor, and viscosities of several ionic liquids were measured at pressures up to 50 MPa⁴² with values reaching $500 \text{ mPa} \cdot \text{s}$ ²⁰ with an uncertainty of $\pm 2\%$, agreeing with the literature.

The vibrating-wire viscometer has many positive qualities: compact, defined uncertainty and not involving exotic materials or procedures. It is surprising that a commercial version has not yet reached market. Vibrating-wire piezometers (for geotechnical applications) and strain gauges have been commercialized for years proving their robustness. There is no reason a robust and practical vibrating-wire viscometer cannot be produced at competitive cost. Several attempts at miniaturizing have been reported, namely one design tailored for a reservoir-fluid storage and transportation vessel,¹⁶ and microfluidic viscometers⁴³ with volume under $20 \mu\text{L}$. The uncertainty in viscosity is $\pm 10\%$, better than expected considering the close proximity of the container walls.⁴³ These minute instruments do not comply with the theoretical specifications of their more accurate predecessors and, in that case, another geometry, like a cantilever⁴⁴ or tuning-fork,⁴ may be easier to fabricate with micro-electro-mechanical techniques.

The main strength of the vibrating-wire viscometer is the availability of a rigorous hydrodynamic model that enables absolute or quasi-absolute measurements. The possibility of simultaneous measurement of density is another advantage. Laboratories in several European countries, in China and in the USA contributed to develop the method, in terms of sensor design, of understanding its operation and extending its applicability. The field of vibrating-wire viscometry is active and promises exciting developments for the future, in academia and in industry.

4.2 Falling Body Viscometer Developments: Small Spheres

DAISUKE TOMIDA AND CHIAKI YOKOYAMA

Falling body methods that are used to measure viscosity include the falling ball, falling sinker, and rolling ball type methods. In recent years, the development of suitable precision measurement instruments has resulted in high precision absolute viscosity measurements using the falling ball method. This chapter describes recent developments in falling body viscometers, and discusses precision viscosity measurement using the falling ball method.

4.2.1 Falling Ball Viscometer

A falling ball viscometer is an instrument used to measure the falling velocity of a ball into a fluid, which is then used to determine the fluid's viscosity using Stokes' law. The viscosity, η , is calculated using:

$$\eta = \frac{d^2(\rho_s - \rho_l)g}{18v}, \quad (4.1)$$

where d is the diameter of the ball, ρ_s is the density of the ball, ρ_l is the density of the sample fluid, g is the local acceleration of the free-fall, and v is the terminal velocity of the falling ball.

However, this equation is only valid if the terminal velocity is reached, and if the ball falls in an unbound medium without inertial effects. We must apply a number of corrections to calculate the experimental terminal velocity. For fall within a cylindrical tube with a diameter D , the correction of the wall effect is given by Faxen⁴⁵ as

$$v_{\text{corr}} = v \left[1 - 2.10444 \left(\frac{d}{D} \right) + 2.08877 \left(\frac{d}{D} \right)^3 - 0.94813 \left(\frac{d}{D} \right)^5 + \dots \right]^{-1}. \quad (4.2)$$

To correct for the inertial effect, Oseen's approximation⁴⁶ in the Navier-Stokes equation gives

$$v_{\text{corr}} = v \left(1 + \frac{3}{16} Re \right)^{-1}, \quad (4.3)$$

where Re is the Reynolds number. A more complete correction due to the inertial effect was derived by Goldstein⁴⁷ as

$$v_{\text{corr}} = v \left(1 + \frac{3}{16} Re - \frac{19}{1280} Re^2 + \frac{71}{20480} Re^3 + \dots \right)^{-1}. \quad (4.4)$$

These last two corrections particularly imply that the Reynolds number of the flow around the ball must be kept very low and it is the satisfaction of

this condition that has eluded many earlier experimenters but has recently been achieved with very small single-crystalline silicon spheres.^{48,49}

The main difficulty when using this method is measuring the velocity of the ball and so the largest contribution to measurement uncertainty comes from the velocity measurement.^{49–51} For this reason we pay particular attention to the techniques associated with that measurement that have been made possible by modern technology.

Mordant and Pinton⁵² developed acoustic measurement systems based on the Doppler effect, using an ultrasonic wave returned by the falling particle. Lommtzsch *et al.*⁵⁰ proposed an alternative optical method in which the ball velocity (U_∞) is determined by the sum of its velocity in the field of the camera (U_{bc}) and the camera velocity (U_c), $U_\infty = U_{bc} + U_c$.

Fujii *et al.*^{48,49} developed an absolute viscosity measurement method based on the falling ball method. They measured the falling velocity of the ball by laser interference tracking using a charge coupled device (CCD) camera. This falling velocity measurement system is shown in Figure 4.3. The z-scan motion of the CCD camera on the motorized stage tracks the falling motion of the ball to keep its image within a few pixels in the captured frames. At the same time, the vertical displacement of the moving camera as a function of time is measured by the laser interferometer, which is synchronized to the shutter timing of the camera. To remove the Abbe error caused by the pitch motion of the Z stage, both the vertical and angular (pitch) displacements of the moving camera are measured simultaneously, using a dual axes laser interferometer. By combining CCD image-processing technology with laser interference tracking technology, the position of the falling ball is measured with an uncertainty of approximately 150 nm.

Brizard *et al.*^{51,53} developed a method that used a line scan CCD camera, as shown in Figure 4.4. The linear camera can obtain very high measurement resolutions and acquisition frequencies, and offers the possibility of taking quasi-instantaneous velocity measurements. This technique can measure the variations in the ball velocity along the tube, and observe its trajectory. Figure 4.5 presents the image of the ball seen by the line scan camera when

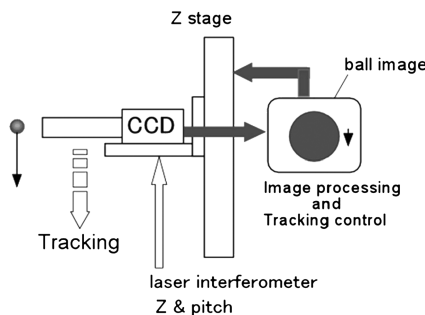


Figure 4.3 Principle of the falling ball viscometer that includes a measurement of the ball velocity.⁴⁹

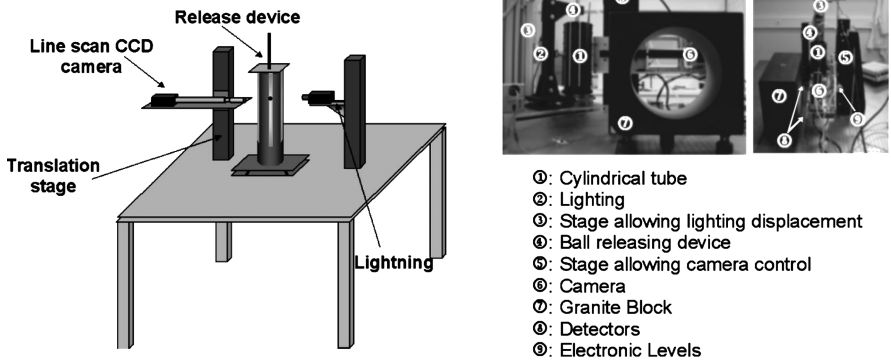


Figure 4.4 Diagram of the experimental set-up for the falling ball velocity measurement using a line scan CCD camera.⁵³

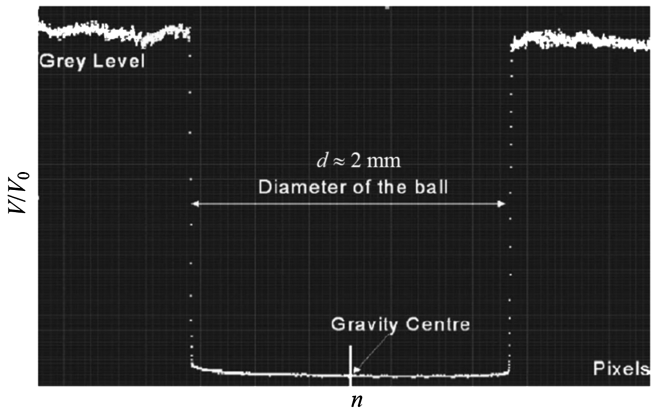


Figure 4.5 The ratio of the voltage V obtained from a charge coupled device (CCD) line-scan camera to an arbitrary reference voltage V_0 as the ball, of diameter $d \approx 2$ mm, passes in front of the lens at the time of release as a function of the number n of pixels; n can be converted to length with a calibration and, in this case, used 2000 pixels with a resolution of 1 pixel to determine the diameter d . The ball edge is determined from the gradient of response between the maximum grey level. These measurements permit the determination of the ball diameter, the barycentric position and, from knowledge of the time interval between two images obtained along a tube of length about 300 mm, the falling ball velocity.⁵³

it passes in front of the lens. The ball edge is where the maximum gradient of the grey level is. This information allows one to measure the ball diameter as well as the barycentric position very accurately. By knowing the time interval between two images and the displacement of the barycenter, we can calculate the falling velocity.

The measurement of the ball's diameter is also one of the largest contributors to the uncertainty. Fujii *et al.*⁴⁸ developed technology that uses a

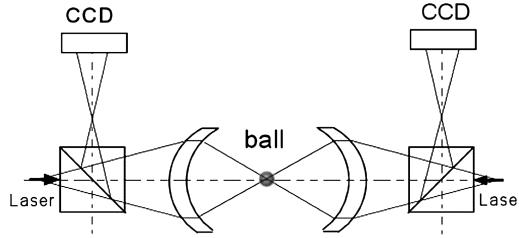


Figure 4.6 Principle of diameter measurement using phase-shifting interferometry with the spherical Fabry–Perot interferometer.⁴⁹

single-crystal-silicon sphere as the falling ball. They used a single-crystal-silicon sphere with a diameter of 2 mm and a mass of approximately 7 mg. They measured the ball diameter using phase-shifting interferometry with the spherical Fabry–Perot interferometer as shown in Figure 4.6. A Fabry–Perot interferometer was then used to measure the diameter of a single-crystal-silicon sphere with a mass of 1 kg and a diameter of 94 mm, with an uncertainty of ± 3 nm.⁵⁴

Feng *et al.*⁵⁵ studied falling ball viscometers in Newtonian fluids using a combination of theoretical analysis, experiments, and numerical simulations. They identified the error sources that affect the accuracy and reproducibility of these tests. They then presented the following recommendations to obtain high precision results.

- Use falling balls that are very consistent in terms of size, sphericity, and surface finish.
- Higher Anti-Friction Bearing Manufacturer’s Association (AFMBA) grade balls provide more consistent results.
- Choose a falling ball and cylinder that result in a small a/D ratio ($a/D \leq 0.05$), which dramatically reduces the off-center error.
- Ensure that the apparatus is vertical and that the ball falls on the vertical axis.
- Multiple trials improve reproducibility and reduce measurement uncertainty.
- Improve the time measurement accuracy.

4.2.2 Falling Sinker-type Viscometer

The falling sinker-type viscometer is often used for precision high pressure viscosity measurements in fluids with high viscosities. Various versions of the experimental apparatus used for this method have been developed. The variations are usually in the methods that detect the passage of the body across the reference positions in the tube, or the exact shape of the falling-body. To perform accurate viscosity measurements using the falling body technique, we must consider various corrections (including the fall-tube

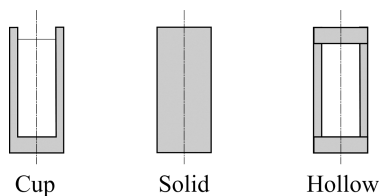


Figure 4.7 Cross-section view of sinker types for high-pressure falling body viscometer.⁵⁷

dimensions, the effects of the fall-tube ends, the terminal velocity, the falling-body shape, and the position of the fall tube).

Daugé *et al.*⁵⁶ used a double tube to prevent any deformation of the inner tube, and measured viscosities at pressures up to 140 MPa. Both tubes contain the sample fluid, and the same pressure conditions exist inside and outside the inner tube.

Bair and Qureshi⁵⁷ used three different kinds of sinkers depending on the sample viscosity, as shown in Figure 4.7. The “solid” sinker has no central flow path and will fall at a velocity of $1 \text{ mm} \cdot \text{s}^{-1}$ for a viscosity of about $0.030 \text{ Pa} \cdot \text{s}$ (as shown in the center of Figure 4.7). The “cup” sinker has similar geometry, but its mass has been reduced by drilling so that it falls at a velocity of $1 \text{ mm} \cdot \text{s}^{-1}$ in a viscosity of $1.7 \text{ mPa} \cdot \text{s}$ (as shown in Figure 4.7). The “hollow” sinker has a central through-hole and falls at a velocity of $1 \text{ mm} \cdot \text{s}^{-1}$ for a viscosity of $5.5 \text{ Pa} \cdot \text{s}$.

Kumagai *et al.*⁵⁸ measured viscosity using a sinker that includes a γ -shaped stabilizer. This ensures that the sinker falls on the central axis. Kumagai *et al.* did not discuss details of the effect of this stabilizer on the viscosity measurements. They measured the viscosity of several mixtures of *n*-alkanes with squalane at temperatures between (273.15 and 333.15) K, and at pressures up to 30 MPa within relative uncertainties of $\pm 2.9\%$.

Sagdeev *et al.*⁵⁹ developed a falling-body viscometer that simultaneously measures the density. They confirmed the accuracy of the method using measurements of pure heptane at temperatures from (298 to 363) K and pressures up to 245 MPa. They measured the density and viscosity of pure polyethylene glycols, and their binary and ternary mixtures at temperatures from (293 to 472) K at atmospheric pressure within $\pm 2.0\%$ uncertainties.

4.3 Rolling Sphere Viscometry in a Diamond Anvil Cell

EVAN H. ABRAMSON

4.3.1 Introduction

Viscosities can be measured^{60–63} in the high-pressure diamond-anvil cell (DAC) by dropping a sphere *through* the fluid, parallel to the two diamond faces, but results have a relative uncertainty of no better than $\pm 30\%$ owing to large wall effects coupled with an inability to release the sphere at precisely controlled distances from the diamonds.

King *et al.*⁶⁴ reasoned that if the sphere were instead allowed to roll down the inclined surface of one of the diamond anvils, the wall effect, although large, might be constant and therefore could be calibrated. Further, the large wall effect afforded by the near diamond would be expected to greatly lessen the relative effects of the far diamond, such that calibration would not be significantly altered by variations in the diamond-to-diamond gap as pressure was changed. Both these suppositions prove to be true.

The method has now been used to measure the shear viscosities of fluids to pressures in excess of 10 GPa and temperatures of 680 K. Viscosities have been recorded from values of 10^{-1} mPa·s up to 10^{10} mPa·s. The large compressions available in the DAC allow the use of density as an (experimentally) independent variable, in studies covering a range from the approximate hard-sphere behaviour of some supercritical fluids, to incipient glassing.

4.3.2 The Rolling Sphere

In a typical arrangement, shown in Figure 4.8, the DAC is tilted with respect to horizontal and a sphere of 30 μm to 70 μm in diameter is allowed to roll down the inner face of the lower diamond. The sphere is imaged onto a high-speed, digital camera and its position recorded as a function of time (Figure 4.9). The images are then analysed to give the terminal speed and, hence, viscosity.

For angles low enough that the sphere will roll (rather than slide) the translational speed v is given by:⁶⁶

$$v = \left[\frac{2\gamma R^2 (\rho_S - \rho_F) g}{9\eta} \right] \{ \sin(\theta) - C \}, \quad (4.5)$$

where R is the sphere radius, ρ_S and ρ_F are the density of sphere and fluid, g the local gravitational acceleration of free fall, and θ the angle with respect to the horizontal. The factor γ , which relates to hydrodynamic forces, is independent of speed, angle and fluid, while C is presumed to derive from frictional forces and is observed to remain constant as the tilt angle changes.

Thus, if the experiment is repeated at several tilt angles, a plot of speed against sine of the angle yields a straight line with the viscosity inversely

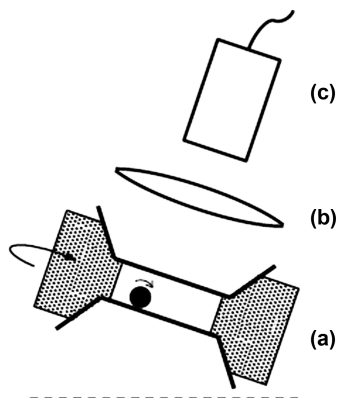


Figure 4.8 Schematic of a rolling sphere experiment. The DAC (a) is tilted, allowing a sphere to roll down the lower diamond face. The fluid is contained by the two diamonds and the steel gasket (stippled areas) into which they are impressed. The DAC can be rotated about an axis normal to the diamond faces, allowing the sphere to be brought to the top. A long-working-distance lens (b) images the contents of the DAC onto a high-speed, digital camera (c).

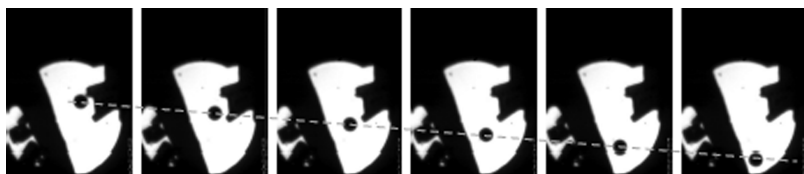


Figure 4.9 Photomicrographs of a back-lit sphere rolling in water,⁶⁵ at 30 ms intervals. The frames encompass a field of $410\ \mu\text{m}$ by $547\ \mu\text{m}$ and the sphere's diameter is $42\ \mu\text{m}$. The two salients machined into the gasket provide means for the sphere to detach itself from the wall. On the left side of the cell, a chamber containing water-soluble pressure markers is isolated by a gold separator. The straight, dashed line through the series of images is drawn as a (rough) indication of constant speed.

proportional to the slope as shown in Figure 4.10. No departure from inverse proportionality between η and the line's slope has been observed for Reynolds numbers, $2\nu R\rho_F/\eta$, ranging from 10^{-3} to 5. This result concurs with findings⁶⁷ for larger spheres (for Reynolds numbers less than 20 a fit of the data gave η proportional to $\nu^{-1.09}$, which is different from the inverse proportionality by less than the uncertainty of the exponent).

Within the theory of a smooth sphere rolling on a smooth plane surface⁶⁹ (see, for example, ref. 70 for a theory of a sphere with asperities), γ is a function solely of the ratio of the sphere's radius to the (presumed) small gap between sphere and surface. Measurements in our group give γ predominantly between 0.11 and 0.13, with outliers between 0.09 and 0.17. King *et al.*⁶⁴ gives $\gamma = 0.12$ to 0.14 for five out of six tests for which the sphere was

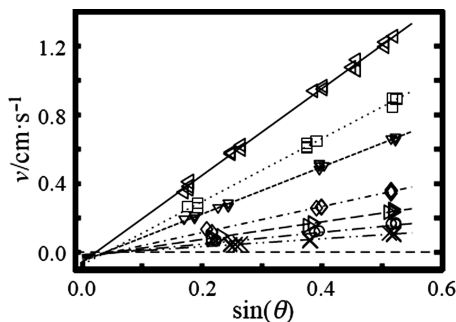


Figure 4.10 Translational speeds are plotted against the sine of the tilt angle for a sphere rolling in nitrogen⁶⁸ at $T = 294$ K. Lines are least-squares fits through the data for each pressure. —, $p = 0.34$ GPa; ···, $p = 0.53$ GPa; - - -, $p = 0.69$ GPa; - · - ·, $p = 1.18$ GPa; - - - -, $p = 1.56$ GPa; - - - - -, $p = 2.02$ GPa; - - - - - -, $p = 2.45$ GPa. Long dashed line indicates $v = 0$. As the viscosity increases with pressure the speeds are seen to decrease correspondingly. Note that the abscissa intercept is non-zero, and that of the lowest pressure data differs significantly from the others.

likely not slipping. Similarly, macroscopic spheres with diameters (2 to 22) mm, of glass, cellulose acetate and poly(methyl 2-methylpropenoate), were found by Carty⁶⁷ to roll with $\gamma = 0.09$ to $\gamma = 0.12$.

Practically, γ is found by rolling the sphere in a fluid of known viscosity, methylbenzene and water being particularly useful as primary calibrants. This is best done with a pressure buffer consisting of an air bubble sealed into the DAC along with the fluid. In the absence of a bubble, errors in calibration develop (*e.g.*, the viscosity of methylbenzene⁷¹ will double due to an accidental increase in pressure from 1 MPa to 100 MPa, which is less than the typical uncertainty of pressure measurement in the DAC). Raising the temperature by several hundred degrees will often result in a persistent change in γ of roughly 10 %, presumably due to modification of one or both surfaces; it is thus prudent to repeat lower temperature measurements occasionally.

Values of C are typically less than 0.10, and have often been assumed to be identically zero. However, even at the relatively large angle of $\theta = 40^\circ$, this assumption can amount to a large error in slope and thus viscosity. Beyond angles of $\approx 40^\circ$ a platinum sphere rolling on diamond has been observed to slip,⁶⁶ and speeds will increase above those given by eqn (4.5).

Viscosities recorded with this technique range from⁷² (0.20 to 10^8) mPa · s;^{64,73,74} modification of the technique to make use of a centrifuge has allowed measurements^{73,75} to 10^{10} mPa · s. Most measurements have been of fluids which tend to glass at higher pressures,^{64,73-76} but there has been at least one investigation of a dilute polymer solution⁷⁷ and several of small, non-glassing molecules,^{64-66,68,78,79} some of the last set taken at pressures up to 10 GPa and temperatures up to 680 K. Such experiments

should be possible at temperatures in excess of 1000 K, limited by the materials and design of the DAC.

4.3.3 Error

Individual measurements of viscosities scatter with relative root-mean-square deviations of $\pm(2$ to $4)\%$. Comparisons with results obtained through other methods of viscometry, in an overlapping pressure range up to ≈ 1 GPa, usually show agreement close to, or within, stated uncertainties.^{64,65,68,78,79} Measurements⁶⁴ of octamethyl trisiloxane at pressures up to 1.3 GPa, extending over seven orders of magnitude in viscosity, agree with previous results within the ± 0.03 GPa uncertainty in the pressure measurement (which, however, propagates to give an uncertainty in viscosity of a factor of 3 at the highest pressures). Larger-than-expected deviations between DAC derived results and those derived from other techniques may be reasonably ascribed to inadequately modelled, pressure-induced strains in the more complex apparatus required by those techniques, particularly at higher temperatures.

For a sphere rolling in a DAC, the geometry of the sphere–surface interaction does not appear to change appreciably over the range of pressures and temperatures surveyed (the exception being the sporadic, and easily observed, change of γ with temperature noted above). For example, two different spheres used in measurements of fluid argon⁷⁹ (Figure 4.11) give the same results at temperatures from 294 K to 673 K, and pressures from 0.1 MPa (in calibrating fluids) to 5 GPa, even as the larger sphere (56 μm diameter) rolls approximately twice as fast as the smaller (38 μm) for any given viscosity and angle. Systematic errors appear to be either less than the scatter or common to all spheres.

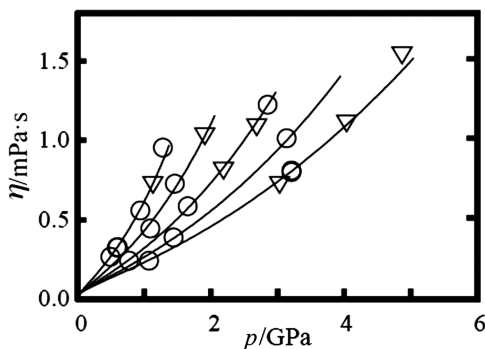


Figure 4.11 Viscosity, η , of argon⁷⁹ as a function of pressure along isotherms (from top to bottom) at temperatures of (294, 373, 473, 573 and 673) K. The curves represent a fit to a modified free-volume equation with four free parameters. \circ , 38 μm diameter sphere; ∇ , 56 μm diameter sphere.

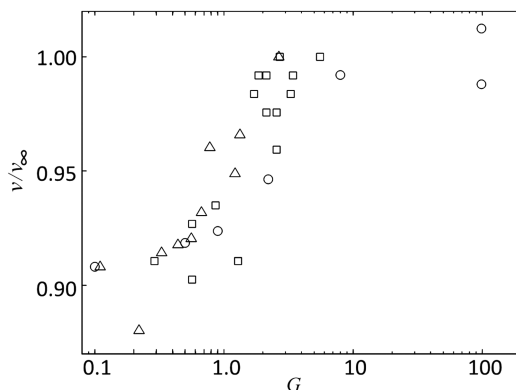


Figure 4.12 The effect on translational speed of the gap between the top of the sphere and the upper diamond surface. Speeds of three different spheres, v , normalized by their values at infinite gap, v_{∞} , are plotted against the ratio (G) of the gap to the sphere diameter. The spheres were rolled in methanol at an angle of $\theta = 30^\circ$. The sphere diameters were as follows: \square , 70 μm ; \triangle , 90 μm ; \circ , 100 μm .

The gap between the top of the sphere and the upper diamond surface will vary with pressure and can be expected to influence the speed of roll. The effect of this parameter,⁶⁶ as Figure 4.12 shows, is small for ratios of gap to sphere diameter, G , between 0.1 and 1.0, more than the normal range of variation required for pressure changes in an experiment.

4.3.4 Experimental Details

In work described in the literature^{65,68,72,78,79} the DAC is held in a temperature-controlled enclosure, itself mounted on a stage capable of rotation about an axis normal to the diamond surfaces. The cell is back-lit and imaged with a microscope (90 mm working distance, $9\times$ working magnification, with a zoom out to $1.4\times$ found useful for alignment) onto a CCD camera (with square pixels, 7.4 micron on a side, in a 640 by 480 array) recording 100 frames per second. The camera's electronic shutter is typically set at 200 μs , making it unnecessary to strobe the illumination (from a small, tungsten-halogen bulb, imaged into the cell). An electrolytic tilt gauge, the light source, rotation stage with mounted oven and cell, microscope, and camera are arrayed on a rigid, hinged beam adjustable from 0° to 90° with respect to the horizontal. With the beam in a horizontal position ($\theta = 90^\circ$) a laser may be focused onto a pressure marker included in the cell and the resulting fluorescence (or Raman scattering) imaged onto a monochromator.

Gasket holes in the DAC are typically between 300 μm and 500 μm in diameter although larger holes, and spheres, have been used in the analogous sapphire-anvil cell.^{80,81} Terminal velocity⁶⁶ is usually achieved within about 0.01 s and decent measurements have been made with roll distances

comparable to the sphere's circumference, although longer rolls are preferred as they allow a better observation of any irregularities.

The sphere may be positioned toward the top of the cell by making use of its adhesion to the gasket edge (and then initiating the roll with a tap), by blocking its roll with another object (*e.g.*, a chip of ruby used for measuring pressure), or simply by rapid rotation of the cell. Occasionally the sphere will roll such as to maintain contact with the edge of the gasket. In such cases it is provident to machine a small projection into the gasket edge, sharp enough to cause the sphere to detach as shown in Figure 4.9.

Adhesive forces between the sphere and diamond surface vary greatly, with load, with load history and, occasionally, across the diamond surface. Sometimes the sphere will roll freely, often it will stick to the gasket edge as the cell is rotated but release with a gentle tap, and other times it cannot be dislodged even with a strong blow to the apparatus. A sphere which is stuck can usually be freed by freezing and then re-melting the fluid. Although such variable behaviour is vexing, it (surprisingly) does not appear to be associated with systematic differences in measured viscosity.

Platinum is particularly useful as a material for the spheres as it is relatively chemically inert and its high density ($21.4 \text{ g} \cdot \text{cm}^{-3}$) requires a less accurate knowledge of the fluid's equation-of-state for buoyancy correction. Within the range of pressures and temperatures for which this technique has so far been used, changes in density⁸² of a Pt sphere require corrections to the calculated viscosity of relatively less than 1%. Spheres have been made either by sprinkling flaked Pt into a flame [*e.g.*, (methane + oxygen)], or in electrical sparks created by intermittently bringing together two Pt wires at $\approx 50 \text{ V}$ ac. In either case, the rain of spheres can be collected and graded (*e.g.*, by allowing them to roll down a microscope slide under ethanol), the best being selected for further use. Scanning electron micrographs of spheres made this way often reveal fissures which don't, however, seem to be a problem.

The tracks of the spheres can be determined easily with image processing software. For each roll, the sphere is found by eye in the first frame and its image defined, the software then searching subsequent frames for the best match. In order to compensate for any vibration of the cell with respect to the camera, the position of the sphere can be indexed with respect to an immobile object (usually a section of the gasket edge or the pressure marker), similarly located for each frame.

4.4 Gas Viscosity-ratio Measurements with Two-capillary Viscometers

ROBERT F. BERG, ERIC F. MAY, AND MICHAEL R. MOLDOVER

4.4.1 Introduction

In this section, we discuss the usefulness of gas viscosity ratios and how to obtain such ratios with single-capillary viscometers. Then, we focus on the two-capillary gas viscometer devised by May *et al.*^{83,84} to measure gas viscosity ratios with very low uncertainties, and subsequently used by Zhang *et al.*⁸⁵ Further details, including a review of four-capillary viscometers and proposals to (i) extend the two-capillary viscometer technique to high pressures, and (ii) measure the water-to-helium viscosity ratio, will be published elsewhere.⁸⁶

The Ar-to-He gas viscosity ratios measured by May *et al.* have proved useful for primary acoustic thermometry⁸⁷ and acoustic redeterminations of the Boltzmann constant.⁸⁸ These acoustic measurements require accurate values of the thermal conductivity of low density argon, which can be obtained by combining the measured Ar-to-He viscosity ratio with theoretical values of helium's viscosity and the Prandtl number for argon. The measured Ar-to-He viscosity ratio also has been used in the temperature range $200\text{ K} < T < 400\text{ K}$ to test *ab initio* calculations of the viscosity and thermal conductivity of argon.^{89,90} The relative uncertainty of the viscosity calculated from the Ar-Ar interatomic potential is estimated to be less than $\pm 0.1\%$ at temperatures as low as 80 K;⁹⁰ however, the uncertainty from the use of classical (rather than quantum-mechanical) calculation has not been quantified.⁸⁷ Thus, low uncertainty gas viscosity-ratio measurements at temperatures below 200 K would be a useful guide to theory. Similar measurements above 400 K would help resolve the current tension between measurements and the theory for the viscosity of hydrogen.⁹¹

The widespread practice of calibrating laminar flow meters with surrogate gases (such as helium or argon) and then using them to meter process gases requires accurate surrogate-to-process gas viscosity ratios.⁹² With this application in mind, Berg and Moldover⁹³ reviewed two hundred viscosity measurements near the reference temperature $T_{\text{ref}} = 298\text{ K}$ and zero density for 11 gases, and determined the viscosity ratios among the gases with a relative uncertainty less than $\pm 0.04\%$, which is smaller than the uncertainty of the separate absolute measurements.⁸⁴ They then anchored the measured viscosity ratios to the remarkably low uncertainty value

$$\eta_{0,T_{\text{ref}}}^{\text{He}} = (19.8253 \pm 0.0002)\mu\text{Pa} \cdot \text{s}, \quad (4.6)$$

calculated *ab initio* by Cencek *et al.*⁹⁴ (using only quantum mechanics, statistical mechanics, and fundamental constants) for helium at a temperature of 298.15 K and zero density. {In eqn (4.6) and the remainder of this section, the superscript is the gas g, the first subscript is the pressure p, and

Table 4.1 Reference viscosities,⁹³ obtained by fitting 235 viscosity ratios measured using 18 instruments. The first column gives the recommended value of $\eta_{0,T_{\text{ref}}}^g$, the viscosity at a temperature of $T_{\text{ref}}=298.15$ K and zero density, and its standard ($k=1$) uncertainty. The value for helium was calculated in ref. 94. The second column gives the corresponding ratios relative to helium. The third column gives the isothermal density derivative of the viscosity that was used to adjust measurements of viscosity to zero density. The fourth column gives the exponent a in the expression $\eta_{0,T}^g = \eta_{0,T_{\text{ref}}}^g (T/T_{\text{ref}})^a$ that was used to adjust $\eta_{0,T_{\text{ref}}}^g$ to T_{ref} . See ref. 93 for details and references.

B	$\frac{\eta_{0,T_{\text{ref}}}^g}{\mu\text{Pa} \cdot \text{s}}$	$\eta_{0,T_{\text{ref}}}^g / \eta_{0,T_{\text{ref}}}^{\text{He}}$	$\frac{10^4(d\eta / d\rho) \cdot \eta^{-1}}{\text{m}^3 \cdot \text{kg}^{-1}}$	a
H ₂	8.8997 ± 0.0030	0.44891 ± 0.00034	19.2 ± 4.7	0.69
He	19.8253 ± 0.0002	1.00000 ± 0.00001	-1.1 ± 1.3	0.69
CH ₄	11.0631 ± 0.0035	0.55803 ± 0.00031	19.2 ± 1.9	0.88
Ne	31.7088 ± 0.0100	1.59941 ± 0.00031	1.4 ± 0.1	0.68
N ₂	17.7494 ± 0.0048	0.89529 ± 0.00027	6.3 ± 0.6	0.77
C ₂ H ₆	9.2305 ± 0.0030	0.46559 ± 0.00033	8.2 ± 2.0	0.94
Ar	22.5666 ± 0.0060	1.13827 ± 0.00027	4.9 ± 0.5	0.85
C ₃ H ₈	8.1399 ± 0.0028	0.41058 ± 0.00035	-4.9 ± 2.0	0.99
Kr	25.3062 ± 0.0080	1.27646 ± 0.00032	3.6 ± 0.5	0.92
Xe	23.0183 ± 0.0072	1.16106 ± 0.00031	2.7 ± 0.2	0.98
SF ₆	15.2234 ± 0.0054	0.76788 ± 0.00036	0.6 ± 0.6	0.89

the second subscript is the temperature.}† Table 4.1 reproduces the viscosities recommended by Berg and Moldover.⁹³

4.4.2 Single-capillary Viscometers

The molar flow rate \dot{n} of a gas through a capillary with internal radius r and length L depends on temperature T and the pressures just upstream (p_1) and downstream (p_2) of the capillary as follows:^{95,96}

$$\dot{n} = \frac{\pi r^4 (p_1^2 - p_2^2)}{16LRT\eta_{0,T}^g} C^g(T, p_1, p_2). \quad (4.7)$$

In eqn (4.7), R is the universal gas constant, and $\eta_{0,T}^g$ is the viscosity determined for a gas g at temperature T in the limit of zero pressure. The first factor in eqn (4.7) comes from combining ideal-gas compressibility with the Hagen–Poiseuille equation for incompressible flow through a capillary,⁹⁷

†Some might prefer the alternate notation illustrated by $\eta(g,p,T) = \eta(\text{He},0,T_{\text{ref}})$.

and it estimates the flow rate to within a few percent for a gas near ambient temperature and pressure. The second factor,

$$C^g(T, p_1, p_2) \equiv \left(1 + \sum_{i=1}^5 c_i^g \right) f_{\text{cent}}(De, r / R_{\text{coil}}), \quad (4.8)$$

contains five terms c_i^g that are usually small corrections to the flow of an ideal gas through a straight capillary. They account for: (1) the density virial coefficients and the viscosity virial coefficient, (2) slip at the capillary wall, (3) the increase in the kinetic energy of the gas as it enters the capillary, (4) gas expansion along the length of the capillary, and (5) the radial temperature distribution within the gas resulting from gas expansion and viscous dissipation. The function f_{cent} accounts for the centrifugal effect that occurs when the capillary is coiled. It depends on the geometric ratio r/R_{coil} , where R_{coil} is the radius of curvature of the capillary coil, and the Dean number $De \equiv (r/R_{\text{coil}})^{1/2} Re$, where $Re \equiv 2M\dot{n}/(\pi r\bar{\eta})$ is the Reynolds number; M is the molar mass, and $\bar{\eta}$ is the viscosity at the average pressure defined by eqn (7) of ref. 95. Further details about each of the correction terms are given in ref. 95.

The most accurate gas viscosity ratios have been measured near room temperature; here we pay special attention to viscosity ratios at $T = 298.15$ K of dilute gases relative to that of helium, which we denote as $\eta_{0,T_{\text{ref}}}^g / \eta_{0,T_{\text{ref}}}^{\text{He}}$. In general, determining $\eta_{0,T_{\text{ref}}}^g / \eta_{0,T_{\text{ref}}}^{\text{He}}$ with a single-capillary viscometer requires measurements, for both gases, of the molar flow rate \dot{n} , the upstream and downstream pressures, and the temperature T of the capillary. One then applies eqn (4.8) twice, once for the test gas and once for helium, and forms the ratio of these two equations:

$$\frac{\eta_{0,T}^g}{\eta_{0,T}^{\text{He}}} = \frac{(p_1^2 - p_2^2)_g}{(p_1^2 - p_2^2)_{\text{He}}} \frac{(1 + \sum_{i=1}^5 c_i^g) f_{\text{cent}}(De_g, r / R_{\text{coil}}) \dot{n}_{\text{He}}}{(1 + \sum_{i=1}^5 c_i^{\text{He}}) f_{\text{cent}}(De_{\text{He}}, r / R_{\text{coil}}) \dot{n}_g}. \quad (4.9)$$

Eqn (4.9) is accurate when the capillary's geometry is consistent with the assumptions used to develop the hydrodynamic model. Three of the corrections in eqn (4.9) are proportional to r/L , so the radius-to-length ratio must be small. If the capillary is straight, small deviations of the capillary bore from circularity and uniformity are acceptable because the effective radius r is determined by fitting to the helium measurement. If a long capillary is wound into a coil, the coil's radius R_{coil} must be sufficiently uniform and well known to accurately calculate the correction function f_{cent} . The correction increases as $\varepsilon(De)^4$, where $\varepsilon \equiv 1 - y/x$ is a measure of the flatness of the capillary, and where x and y are the bore's (unknown) semi-radii.^{84,95,96}

Eqn (4.9) includes a correction for slip flow that is proportional to the ratio of the mean free path to the capillary's radius: λ/r , where λ is the mean free path. The calculated correction assumes $\lambda/r \ll 1$. Helium requires special attention because, for a given temperature and pressure, its mean free path is the largest of any gas. More importantly, the momentum accommodation

coefficient for helium on smooth quartz glass deviates from unity and was observed to drift from year to year in the same capillary.⁹⁵

Another effect sensitive to λ/r is the thermomolecular pressure gradient⁹⁸ that can occur when there is a large difference between the temperatures of the capillary and the pressure sensors. Not accounting for this effect will cause errors in p_1 and p_2 at sufficiently low pressures.

Determining $\eta_{0,T_{\text{ref}}}^g/\eta_{0,T_{\text{ref}}}^{\text{He}}$ with a single-capillary viscometer requires a flow meter with a nonlinearity and irreproducibility that are smaller than the desired uncertainty of the viscosity ratio. The flow meter's absolute uncertainty is less important because an incorrect calibration factor will cancel out of the factor $\dot{n}_{\text{He}}/\dot{n}_g$ in eqn (4.9) and affect only the corrections that are proportional to Re and De , where De is the Dean number.

4.4.3 Two-capillary Viscometers

A two-capillary viscometer, comprising two capillaries in series, can be used to measure the temperature dependence of viscosity ratios with small uncertainty and without the need for a flow meter. May *et al.*^{83,84} developed and used such a viscometer to measure the viscosities of hydrogen, methane, argon, and xenon in the temperature range from 200 K to 400 K. They analysed their measurements with the relation,

$$\eta_{0,T}^g = \eta_{0,T_{\text{ref}}}^{\text{He}} \left(\frac{\eta_{0,T}^{\text{He}}}{\eta_{0,T_{\text{ref}}}^{\text{He}}} \right)_{\text{ab initio}} \left(\frac{\eta_{0,T_{\text{ref}}}^g}{\eta_{0,T_{\text{ref}}}^{\text{He}}} \right) R_{T,T_{\text{ref}}}^{\text{g,He}}. \quad (4.10)$$

Eqn (4.10) has four factors: (i), a reference value $\eta_{0,T_{\text{ref}}}^{\text{He}}$ for the viscosity of helium at zero density and 298.15 K, calculated *ab initio* from quantum mechanics and statistical mechanics;⁹⁴ (ii), the temperature-dependent ratio $(\eta_{0,T}^{\text{He}}/\eta_{0,T_{\text{ref}}}^{\text{He}})_{\text{ab initio}}$, also calculated *ab initio*;⁹⁴ (iii), a reference value for the viscosity ratio $\eta_{0,T_{\text{ref}}}^g/\eta_{0,T_{\text{ref}}}^{\text{He}}$ measured at 298.15 K;⁹³ and (iv), a measurement of the temperature-dependent ratio of viscosity ratios,

$$R_{T,T_{\text{ref}}}^{\text{g,He}} \equiv \left(\frac{\eta_{0,T}^g}{\eta_{0,T}^{\text{He}}} \right) / \left(\frac{\eta_{0,T_{\text{ref}}}^g}{\eta_{0,T_{\text{ref}}}^{\text{He}}} \right). \quad (4.11)$$

May *et al.*^{83,84} used a single-capillary viscometer to measure $\eta_{0,T_{\text{ref}}}^g/\eta_{0,T_{\text{ref}}}^{\text{He}}$ and a two-capillary viscometer to measure $R_{T,T_{\text{ref}}}^{\text{g,He}}$. Such an approach is effective because the uncertainties of the theoretical quantities $\eta_{0,T}^{\text{He}}$ and $(\eta_{0,T}^{\text{He}}/\eta_{0,T_{\text{ref}}}^{\text{He}})_{\text{ab initio}}$ are less than $\pm 0.01\%$ ⁹⁴ and because the uncertainties of the measured values of the ratios $\eta_{0,T_{\text{ref}}}^g/\eta_{0,T_{\text{ref}}}^{\text{He}}$ and $R_{T,T_{\text{ref}}}^{\text{g,He}}$ are nearly equal to their precisions.

The reference ratio $\eta_{0,T_{\text{ref}}}^g/\eta_{0,T_{\text{ref}}}^{\text{He}}$ was measured by a single-capillary viscometer using the techniques and analysis described in ref. 83, 84 and 95, while $R_{T,T_{\text{ref}}}^{\text{g,He}}$ was measured over the temperature range of interest by the two-capillary viscometer shown in Figure 4.13. With the upstream capillary's temperature controlled at the reference temperature of 298.15 K, and the

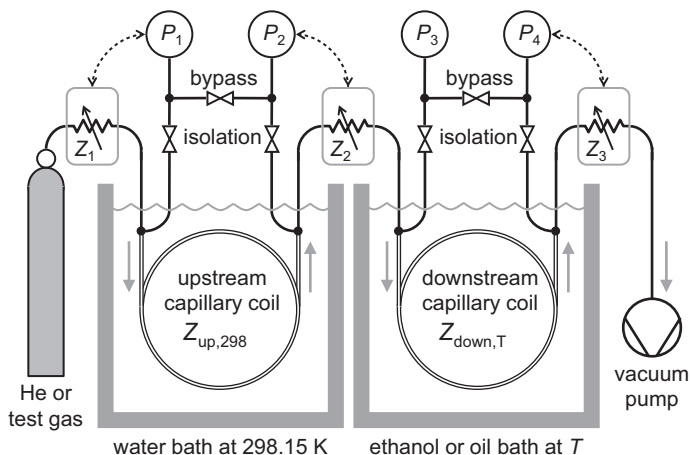


Figure 4.13 Schematic diagram of the two-capillary viscometer used by May *et al.*^{83,84} The impedances Z_{up} and Z_{down} were coiled nickel capillaries with a length of 7 m and an inside diameter of 0.8 mm. The variable impedances Z_1 and Z_3 were piezoelectric gas leak valves, and Z_2 was either a leak valve or a mass flow controller. (Reprinted from ref. 83 with permission of Springer.)

downstream capillary's temperature controlled at the measurement temperature T , helium and the test gas were flowed alternately through the two-capillary viscometer while the pressures were measured at the ends of both capillaries. Importantly, no flow rate measurements were required to determine $R_{T,T_{\text{ref}}}^{\text{g,He}}$.

Figure 4.13 indicates five flow impedances: the upstream and downstream capillaries, denoted respectively as $Z_{\text{up},T_{\text{ref}}}$ and $Z_{\text{down},T}$, each of which is connected to an upstream and downstream pressure gauge, and the variable impedances denoted as Z_1 , Z_2 and Z_3 . During a measurement p_1 and p_2 were maintained at constant, predetermined values by controlling Z_1 and Z_2 . This established a stable but unknown gas flow rate \dot{n} that was identical through both capillaries. If both \dot{n} and $Z_{\text{down},T}$ were known, eqn (4.7) could be used to determine the viscosity at the temperature T from accurate measurements of p_3 and p_4 . However, \dot{n} and $Z_{\text{down},T}$ were unknown; therefore, eqn (4.7) was applied separately to the upstream and downstream capillaries to eliminate \dot{n} and obtain an expression for the viscosity ratio $\eta_{0,T}^{\text{g}}/\eta_{0,T_{\text{ref}}}^{\text{g}}$ in terms of p_1 , p_2 , p_3 and p_4 . Combining that expression for the test gas with a similar expression for the helium measurements yields the working equation:

$$R_{T,T_{\text{ref}}}^{\text{g,He}} = \frac{(p_3^2 - p_4^2)^{\text{g}} (p_1^2 - p_2^2)^{\text{He}} C^{\text{g}}(T, p_3, p_4) C^{\text{He}}(T_{\text{ref}}, p_1, p_2)}{(p_1^2 - p_2^2)^{\text{g}} (p_3^2 - p_4^2)^{\text{He}} C^{\text{He}}(T, p_3, p_4) C^{\text{g}}(T_{\text{ref}}, p_1, p_2)}. \quad (4.12)$$

Eqn (4.12) does not contain the impedance ratio $Z_{\text{up},T_{\text{ref}}}/Z_{\text{down},T_{\text{ref}}}$, which depends on temperature through the thermal expansion of the downstream capillary. Instead, eqn (4.12) contains the viscosity ratio $\eta_{0,T}^{\text{He}}/\eta_{0,T_{\text{ref}}}^{\text{He}}$, which is

known from *ab initio* calculations. The dimensions of the capillaries appear only in the correction terms of eqn (4.8); therefore, approximate values of the dimensions are sufficient for eqn (4.12). May *et al.*^{83,84} used two coils of electroformed nickel tubing, each with a nominal internal diameter of 0.762 mm, a length of about 7.45 m, in a helical coil with a 0.1 m radius of curvature and a length of 0.04 m.

Stability and accurate measurements of temperature and pressure are central to the determinations of $\eta_{0,T_{\text{ref}}}^{\text{g}}/\eta_{0,T_{\text{ref}}}^{\text{He}}$ and $R_{T,T_{\text{ref}}}^{\text{g,He}}$. The nickel capillaries used by May *et al.*^{83,84} were immersed in stirred liquid baths that controlled their temperatures with an uncertainty of ± 0.01 K. The flow rates and the viscometer's design ensured that the temperature of the flowing gas reached the bath's temperatures before the gas entered each capillary. The pressure transducers had full scales of 300 kPa or 150 kPa, an uncertainty of ± 0.008 % of full scale (± 24 Pa or ± 12 Pa), and a resolution of 0.16 Pa. The experimental quantities of primary importance are the difference pressures across the capillaries, $\Delta p_{12} \equiv p_1 - p_2$ and $\Delta p_{34} \equiv p_3 - p_4$. Several refinements were used to measure Δp_{12} and Δp_{34} with relative uncertainties of order $\pm 10^{-4}$. The two pairs of transducers (which measured p_1 , p_2 , p_3 and p_4) and the two bypass valves were housed in a temperature controlled enclosure. Before and after every measurement, the bypass valves were opened to measure the zero-offsets of Δp_{12} and Δp_{34} near the average operating pressures. The measured zero-offsets were used to tare subsequent readings of Δp_{12} and Δp_{34} made while the bypass valves were closed. The pressures p_1 , p_2 and p_4 were controlled at their set points using the variable impedances Z_1 , Z_2 and Z_3 and digital proportional-integral algorithms. The pressure set-points were chosen so that for both gases the flow rates and average pressures within the two capillaries were similar. The upstream capillary's upstream pressure p_1 was usually fixed near 125 kPa, and its downstream pressure p_2 was set to four values (between about 100 kPa and 120 kPa) to produce four flow rates ranging from about $4 \mu\text{mol} \cdot \text{s}^{-1}$ to $80 \mu\text{mol} \cdot \text{s}^{-1}$. The downstream capillary's downstream pressure p_4 was then controlled sequentially at six set points between 13 kPa and 75 kPa for each of the four flow rates. This array of 24 measurements per gas per temperature was used to estimate the dependence of the measured values of $R_{T,T_{\text{ref}}}^{\text{g,He}}$ [eqn (4.12)] on the Dean number De and the small pressure-dependence of the viscosity, as described below. Automation of the entire apparatus and experimental method, including taring of the pressure transducers was essential because the measurements of $R_{T,T_{\text{ref}}}^{\text{g,He}}$ at each temperature required a time of several hours while the apparatus stepped through two identical sets of $[p_2, p_4]$ conditions, one for helium and one for the test gas. These refinements to the apparatus and experimental method enabled the pressure differences Δp_{12} and Δp_{34} to be controlled and measured to within ± 0.01 %, with the dominant uncertainty due to the instability (≈ 2 Pa) in the uncontrolled pressure p_3 .

In many cases the correction factor $C^{\text{g}}(T, p_1, p_2)$ can be determined with sufficient accuracy that eqn (4.12) can be used directly to calculate $R_{T,T_{\text{ref}}}^{\text{g,He}}$. Such cases require that (a) the Dean number and, hence, the centrifugal flow

correction be sufficiently small, and (b) that the following parameters required to evaluate the c_i^g terms for the gas are sufficiently well known: the molar mass M , the zero-density viscosity $\eta_{0,T}^g$, the density virial coefficients B and C , the thermal conductivity, the temperature derivative of the zero-density viscosity $d\eta_{0,T}^g/dT$, and the viscosity virial coefficient $B_\eta \equiv \lim_{\rho \rightarrow 0} (\partial\eta/\partial\rho)_T$. Of these, it is B_η that is least well known, but under certain circumstances the equivalent quantity $b_T^g \equiv \lim_{p \rightarrow 0} (\partial\eta/\partial p)_T/\eta = B_\eta(\partial\rho/\partial p)_T/\eta$ can be measured with a modest uncertainty by the two-capillary viscometer itself.

To determine whether the correction terms in $C^g(T, p_1, p_2)$ are sufficiently accurate, it is useful to calculate the quantity

$$\Xi^g(T) \equiv \frac{\Delta p_{34} \bar{p}_{34} C^g(T, p_3, p_4)}{\Delta p_{12} \bar{p}_{12} C^g(T_{\text{ref}}, p_1, p_2)}, \quad (4.13)$$

and test its dependencies on the mean pressure in the downstream capillary, $\bar{p}_{34} \cong (p_3 + p_4)/2$ and on the Dean number of the flow through the downstream capillary. An incorrect value of B_η will cause Ξ^g to vary with \bar{p}_{34} . May *et al.*⁸³ adjusted B_η to minimize such variation, and thereby obtained a more accurate value of B_η .

For gases that have accurately-known density and viscosity virial coefficients, the pressure-dependence of Ξ^g can be taken into account when calculating the correction terms c_i^g . However, accounting for the dependence of Ξ^g on the Dean number is more complicated. The correction for centrifugal flow in the hydrodynamic model extends to $De > 16$ only if the capillary bore is sufficiently circular and uniform. Capillaries that are robust enough to operate over a wide range of temperatures are unlikely to satisfy this criterion, and the lowest order correction to the centrifugal function f_{cent} in eqn (4.7) for a capillary with a slightly elliptical bore is proportional to $(De)^4$ (ref. 83,84,95,96). Under these circumstances, the value of $R_{T,T_{\text{ref}}}^{\text{g,He}}$ should not be estimated directly from eqn (4.12) but rather from

$$R_{T,T_{\text{ref}}}^{\text{g,He}} = \lim_{De \rightarrow 0} \Xi^g(T) / \lim_{De \rightarrow 0} \Xi^{\text{He}}(T). \quad (4.14)$$

4.5 Sealed Gravitational Capillary Viscometers for Volatile Liquids

ARNO LAESECKE

4.5.1 Introduction

In 1991, Kawata *et al.*⁹⁷ reviewed the metrology with open gravitational capillary viscometers, but there has been no review of sealed instruments for volatile liquids. At that time, such instruments were increasingly used to determine the viscosity of alternative refrigerants, which might be used to replace the ozone-depleting chlorofluorocarbons.⁹⁹ Comparisons with viscosities that were measured with other types of viscometers showed systematic and unexpectedly large deviations, in one case even greater than 30%.¹⁰⁰ These discrepancies were resolved in and reported by NIST.^{101,102} Measurements with **sealed** gravitational capillary viscometers had been analyzed with the working equations for **open** gravitational capillary viscometers because of a gap in reference texts and standards. From its beginnings with Hagen, Poiseuille, and Hagenbach,¹⁰³ capillary viscometry had been predominantly performed with open instruments on non-volatile liquids. Applications of the technique to volatile liquids were sporadic until the new class of chlorofluorocarbon refrigerants led to the expansion of the refrigeration and air-conditioning industries in the 1950s. However, reference texts and standards for sealed instruments to recognize their distinct differences from open capillary viscometers were not developed in parallel with their more frequent use.

This section fills this gap. Section 4.5.2 gives an overview of the evolution of sealed gravitational capillary viscometers. Section 4.5.3 discusses the vapor buoyancy correction that applies to all sealed instruments. Section 4.5.4 addresses the radial acceleration correction that is needed if the capillary is curved or coiled. As with most corrections to viscosity measurements, their omission yields systematically too high results.

4.5.2 Instruments

Three types of sealed gravitational capillary viscometers were developed: (1), instruments made out of thick-walled glass; (2), open capillary viscometers enclosed in metallic pressure vessels; and (3), compact instruments made out of stainless steel. Edwards and Bonilla¹⁰⁴ constructed in 1944 a sealed viscometer of type 1. To achieve sufficiently high flow impedance for sufficiently long efflux times, the capillary with an inner diameter of 0.57 mm was wound in a coil with three turns. Over the next 46 years, this instrument served as an example for the studies of Mears *et al.*,¹⁰⁵ Phillips and Murphy^{106,107} and of Shankland *et al.*^{108,109} Except for the data of Edwards and Bonilla, the results of these measurements with sealed viscometers with coiled capillaries were later found to be up to 33 % higher than data that were determined with other techniques.

Sealed viscometers of type 2 were first employed by Eisele *et al.*¹¹⁰ and then by Gordon *et al.*¹¹¹ The working equation of Cannon *et al.*¹¹² for open capillary viscometers was quoted for this sealed instrument. Kumagai and Takahashi¹¹³ constructed type 1 sealed viscometers but with straight vertical capillaries and quoted also the working equation for open capillary viscometers. They showed that some data of Gordon *et al.*¹⁰⁹ deviated systematically with temperature up to $\pm 8\%$ from theirs. The results of Kumagai and Takahashi¹¹³ were later also found to exceed literature data systematically with temperature by up to 17%. Han *et al.*^{114,115} adopted the type 2 viscometer design and used capillaries with internal diameters from 0.110 mm to 0.370 mm. Measurement results from this instrument agreed with the results of Kumagai and Takahashi¹¹³ and with some literature data, while there were systematic deviations of more than $\pm 10\%$ from other data sets. Viscometry seemed to have a major problem.

The third type of sealed capillary viscometer was developed by Ripple at NIST.¹¹⁶ The first implementation had a one-coil capillary with an internal diameter of 0.508 mm.¹¹⁶ The second instrument with a straight vertical capillary is shown with its dimensions in Figure 4.14. Both instruments differed from the previously discussed sealed viscometers in that the flow

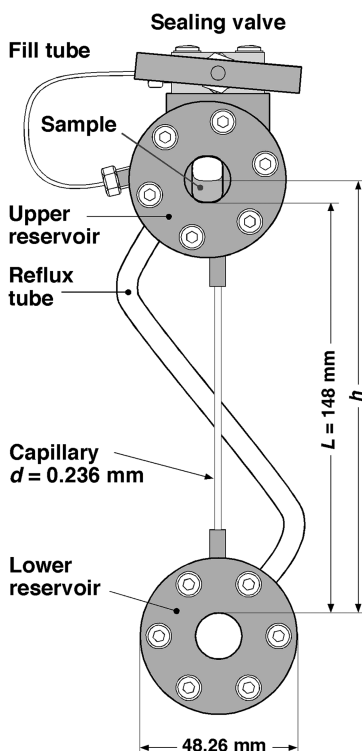


Figure 4.14 Sealed gravitational capillary viscometer with straight vertical capillary developed at NIST.¹⁰¹

rate of the sample was not determined by measuring an efflux time interval t between two marks at the upper reservoir but by observing the descent of the liquid meniscus in that part of the instrument at several levels h to obtain the rate $\dot{h} = dh/dt$. Using this quantity requires a modified working equation for this viscometer.^{102,117} Cousins and Laesecke¹¹⁸ described details of the experimental determination of \dot{h} and the associated uncertainty.

Ripple and Defibaugh¹⁰¹ pointed out that some of the literature data obtained in sealed gravitational capillary viscometers were analyzed without accounting for the vapor buoyancy. They detailed this contribution for the liquids they had measured and showed that correcting for this effect led to a remarkable consistency between their experimental results and the originally deviating literature data. This aspect was investigated further by Laesecke *et al.*¹⁰² with measurements of ammonia, 1,1,1,2-tetrafluoroethane (known by the refrigeration nomenclature as R134a), and difluoromethane (R32) in the same instrument. In addition, the effect of radial acceleration on flow in coiled capillaries was quantified and demonstrated to exceed that of the vapor buoyancy at certain conditions. Accounting for the vapor buoyancy in sealed instruments and for the radial acceleration in those with coiled capillaries reconciled all originally deviating viscosity measurements in gravitational capillary viscometers with the results measured with other instruments. Even the strong deviations of the data of Phillips and Murphy,^{106,107} which had been inexplicable for nearly three decades, could be reconciled. The papers of Ripple and Defibaugh¹⁰¹ and Laesecke *et al.*¹⁰² prompted Kumagai and Yokoyama¹¹⁹ to publish vapor buoyancy-corrected values of the viscosity data for eleven liquids that had been published in 1991.¹¹³

Owing to the infrequent use of sealed instruments, published working equations for gravitational capillary viscometers had often been simplified by neglecting the influence of the gas above the liquid on the driving pressure head of the efflux. One exception is the working equation reported by Wedlake *et al.*:¹²⁰

$$\eta = c_0(\rho_L - \rho_V)\Delta t - b\rho_L/\Delta t + c_1\gamma\Delta t. \quad (4.15)$$

The dynamic viscosity η depends on the density of the liquid ρ_L and that of the vapor or gas above the liquid, ρ_V , as well as the surface tension γ between the liquid and the gas. The measurand is the efflux time interval Δt that elapses when a known volume of liquid drains through the capillary. The constants c_0 , c_1 , and b are determined by calibration with viscosity standards. The first term in eqn (4.15) is the Hagen–Poiseuille term, which describes the flow of the liquid through the capillary. The second term is the correction for the kinetic energy dissipation in the liquid at the inlet and outlet of the capillary.⁹⁷ The third term is a correction for the effects of surface tension at the walls of the capillary.^{102,118,120} As mentioned before, the working eqn (4.15) has to be modified for the sealed NIST viscometers

because the rate of descent of the liquid meniscus \dot{h} is measured rather than an efflux time interval Δt . Then, the dynamic viscosity is obtained from

$$\eta = c_0(\rho_L - \rho_V)/\dot{h} - B\rho_L\dot{h} + C_1\gamma/\dot{h}, \quad (4.16)$$

with the revised calibration constants C_0 , C_1 , and B .¹²¹ Much of the confusion about the systematic deviations of viscosity data obtained with sealed capillary viscometers arose because they had been soundly calibrated with the only available reference liquids, which were non-volatile. Viscometers that are intended for measurements of volatile liquids should be calibrated with volatile reference standards to ensure their uncertainty at the intended operating conditions. Using such reference materials would likely also reduce the difference in surface tension between the calibration liquid and the liquids to be measured, because their chemical structures might be more similar. Wedlake *et al.*¹²⁰ noted that residual surface tension errors for open gravitational capillary viscometers may be as large as $\pm 0.4\%$. Calibration with volatile reference standards would therefore reduce the overall measurement uncertainty of sealed gravitational capillary viscometers by at least this amount. For this reason, Cousins and Laesecke¹¹⁸ used pentane as calibration liquid. Unlike viscosity standards for open capillary viscometers, which are handled in ambient air, those for sealed instruments will be disseminated in pressure vessels due to their volatility and thus may be polar and hygroscopic. Laesecke *et al.*¹⁰² proposed three fluorinated compounds as possible reference standards for sealed capillary viscometers. The characterization of such reference standards requires saturated vapor density as well as surface tension and the viscosity and density of the saturated liquid. Nevertheless, broadening viscosity reference standards to those that are volatile at ambient conditions and have lower viscosities than $0.3 \text{ mPa} \cdot \text{s}$ at 298 K would be valuable for lower uncertainty viscometry in general.

4.5.3 Vapor Buoyancy Correction

Sealed viscometers have to be evacuated before the sample liquid is admitted into the instrument. Depending on its volatility, the sample can be drained from a reservoir or condensed into the instrument by cooling the viscometer. When a sufficient volume of sample has been introduced, the instrument is sealed off and from this point on saturated liquid and saturated vapor are in phase equilibrium. With increasing temperature, the saturated vapor density ρ_{SV} increases and the saturated liquid density ρ_{SL} decreases. The latter reduces the driving pressure head and the former exerts buoyancy, which has to be accounted for in the first terms of eqn (4.15) and (4.16) by the density difference.

The vapor buoyancy correction may be considerable. For 1,1,1-trifluoroethane (given the acronym R143a by the refrigeration community), Kumagai and Yokoyama¹¹⁹ applied this correction and obtained a 17% lower viscosity at 323 K. Even a correction of only $\pm 1\%$ should not be

considered negligibly small. After all, this is twice that of previously mentioned surface tension effects and the uncertainty of the vapor buoyancy correction is smaller than the correction itself.^{102,118} The vapor buoyancy correction has been increasingly considered in measurements with sealed gravitational capillary viscometers^{122–124} but exceptions have occurred.¹²⁵

Measurements of mixtures in sealed gravitational capillary viscometers differ significantly from measurements in open viscometers because the composition of the saturated liquid and vapor changes with temperature as more volatile components evaporate preferably. Because it is not feasible to draw liquid or vapor samples from a sealed viscometer during the measurements, the compositions of the two phases at the measurement temperatures have to be estimated by an equation of state or Helmholtz function for the sample mixture. This requires the bulk density of the mixture in the viscometer which has to be determined during mixture preparation¹¹⁷ or from the internal volume of the viscometer and the sample mass by weighing the viscometer before and after filling.¹²⁶ If the composition dependence of the mixture viscosity is substantial as in systems of nonpolar and polar components, the uncertainty of the mixture viscosity measurement may be significantly higher than for pure fluids.

4.5.4 Radial Acceleration Correction

In curved or coiled tubes, the resistance to flow increases because the radial acceleration of the liquid or gas causes transverse flow. A correction for the radial acceleration is required to determine accurate viscosities. Although coiled capillaries have been used in viscometry for decades, the review of Kawata *et al.*⁹⁷ did not address radial acceleration. Often, the earliest studies of the late 1920s are quoted although these corrections have been found to be inadequate,^{102,127,128} and Berger *et al.*¹²⁹ reviewed numerous later studies. The most recent and accurate correction function for flow rates in coiled capillaries was given by Berg⁹⁵ as $f_{\text{cent}}(De, \delta)$ in terms of the Dean number $De \equiv Re\delta^{1/2}$, with the Reynolds number Re , and the ratio $\delta = (r/R_{\text{coil}})$, where r is the internal radius of the capillary, and R_{coil} is the radius of the coil. This correction was discussed in section 4.4.2. When coiled capillaries are used in sealed viscometers, these correction functions have to be applied to the first two terms of the working eqn (4.15) so that

$$\eta = f_{\text{cent}}[c_0(\rho_{\text{SL}} - \rho_{\text{SV}})\Delta t - b\rho_{\text{L}}/\Delta t] + c_1\gamma\Delta t, \quad (4.17)$$

and accordingly in eqn (4.16). Berg⁹⁵ discussed the correction functions for Dean numbers up to 114 while many measurements with sealed gravitational capillary viscometers had been carried out at Dean numbers up to 35.¹⁰² The importance of the radial acceleration correction must not be underestimated. The magnitude of the correction in sealed gravitational capillary viscometers for liquids is exemplified in Figure 4.15 which shows percent deviations of the viscosity data of Shankland *et al.*¹⁰⁹ and Kumagai and Takahashi¹¹³ for R134a from the correlation of Huber *et al.*¹³⁰

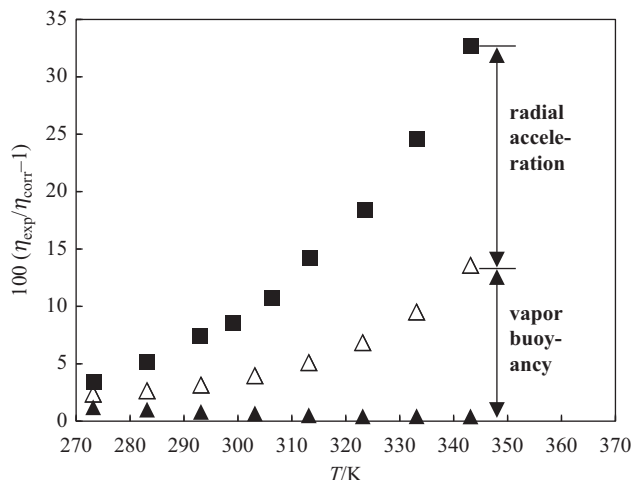


Figure 4.15 Fractional deviations of the measured viscosity, η_{exp} , for 1,1,1,2-tetrafluoroethane (R134a) from the correlation of Huber *et al.*,¹³⁰ η_{corr} , as a function of temperature T . ■, Shankland *et al.*¹⁰⁹; Δ, Kumagai and Takahashi^{113,119}; ▲, Kumagai and Takahashi^{113,119} vapor-buoyancy corrected results.

Shankland *et al.*¹⁰⁹ used a sealed viscometer with a coiled capillary while Kumagai and Takahashi¹¹³ used a sealed instrument with a straight vertical capillary. Their data require only the vapor buoyancy correction which reduces the deviation at 343 K from $\pm 13.6\%$ to $\pm 0.4\%$. The data point of Shankland *et al.*¹⁰⁹ at this temperature deviates by $\pm 32.7\%$. The difference to the deviation of the corresponding uncorrected data point of Kumagai and Takahashi is $\pm 19.1\%$ and is due to the radial acceleration.

References

1. J. T. Tough, W. D. McCormick and J. G. Dash, *Rev. Sci. Instrum.*, 1964, **35**, 1345.
2. *Experimental Thermodynamics. Vol. III. Measurement of the Transport Properties of Fluids*, ed. W. A. Wakeham, A. Nagashima and J. V. Sengers, Blackwell Scientific Publications, Oxford, 1991.
3. V. Majer and A. A. H. Padua, *Experimental Thermodynamics VI: Measurement of the Thermodynamic Properties of Single Phases*, IUPAC-Elsevier, 2003.
4. D. I. Bradley, M. Človečko, S. N. Fisher, D. Garg, A. M. Guénault, E. Guise, R. P. Haley, G. R. Pickett, M. Poole and V. Tsepelin, *J. Low Temp. Phys.*, 2012, **171**, 750.
5. P. S. van der Gulik, R. Mostert and H. R. van den Berg, *Physica A*, 1988, **151**, 153.

6. T. Retsina, S. M. Richardson and W. A. Wakeham, *Appl. Sci. Res.*, 1986, **43**, 127.
7. T. Retsina, S. M. Richardson and W. A. Wakeham, *Appl. Sci. Res.*, 1987, **43**, 325.
8. A. A. H. Padua, J. M. N. A. Fareleira, J. C. G. Calado and W. A. Wakeham, *Rev. Sci. Instrum.*, 1998, **69**, 2392.
9. F. Guillon, S. Hubert and I. L'Heureux, *Physica B*, 1994, **194–196**, 155.
10. F. Ciotta and J. P. M. Trusler, *J. Chem. Eng. Data*, 2010, **55**, 2195.
11. M. J. Assael and S. K. Mylona, *J. Chem. Eng. Data*, 2013, **58**, 993.
12. F. Audonnet and A. A. H. Padua, *Fluid Phase Equil.*, 2001, **181**, 147.
13. F. J. P. Caetano, J. M. N. A. Fareleira, C. M. B. P. Oliveira and W. A. Wakeham, *J. Chem. Eng. Data*, 2005, **50**, 1875.
14. F. Peleties and J. P. M. Trusler, *J. Chem. Eng. Data*, 2011, **56**, 2236.
15. M. E. Kandil, K. N. Marsh and A. R. H. Goodwin, *J. Chem. Eng. Data*, 2005, **50**, 647.
16. D. R. Caudwell, A. R. H. Goodwin and J. P. M. Trusler, *J. Petroleum Sci. Eng.*, 2004, **44**, 333.
17. P. L. Woodfield, A. Seagar and W. Hall, *Int. J. Thermophys.*, 2012, **33**, 259.
18. D. R. Caudwell, J. P. M. Trusler, V. Vesovic and W. A. Wakeham, *Int. J. Thermophys.*, 2004, **25**, 1339.
19. F. J. P. Caetano, J. L. C. Mata, J. M. N. A. Fareleira, C. M. B. P. Oliveira and W. A. Wakeham, *Int. J. Thermophys.*, 2004, **25**, 1.
20. J. C. F. Diogo, F. J. P. Caetano, J. M. N. A. Fareleira, W. A. Wakeham, C. A. M. Afonso and C. S. Marques, *J. Chem. Eng. Data*, 2012, **57**, 1015.
21. J. Wilhelm, E. Vogel, J. K. Lehmann and W. A. Wakeham, *Int. J. Thermophys.*, 1998, **19**, 391.
22. P. S. van der Gulik and N. J. Trappeniers, *Physica A*, 1986, **135**, 1.
23. M. J. Assael, C. M. B. P. Oliveira, M. Papadaki and W. A. Wakeham, *Int. J. Thermophys.*, 1992, **13**, 593.
24. I. Etchart, M. Sullivan, J. Jundt, C. Harrison, A. R. H. Goodwin and K. Hsu, *J. Chem. Eng. Data*, 2008, **53**, 1691.
25. M. Sullivan, C. Harrison, A. R. H. Goodwin, K. Hsu and S. Godefroy, *Fluid Phase Equil.*, 2009, **276**, 99.
26. M. J. Assael, M. Papadaki, M. Dix, S. M. Richardson and W. A. Wakeham, *Int. J. Thermophys.*, 1991, **12**, 231.
27. D. Seibt, S. Herrman, E. Vogel, E. Bich and E. Hassel, *J. Chem. Eng. Data*, 2009, **54**, 2626.
28. A. A. H. Padua, J. M. N. A. Fareleira, J. Calado and W. A. Wakeham, *Int. J. Thermophys.*, 1994, **15**, 229.
29. A. R. H. Goodwin and K. N. Marsh, *J. Chem. Eng. Data*, 2011, **56**, 167.
30. M. J. Assael, H. M. T. Avelino, N. K. Dalaouti, J. M. N. A. Fareleira and K. R. Harris, *Int. J. Thermophys.*, 2001, **22**, 789.
31. K. R. Harris, *J. Chem. Eng. Data*, 2009, **54**, 2729.
32. F. Ciotta, G. Maitland, M. Smietana, J. P. M. Trusler and V. Vesovic, *J. Chem. Eng. Data*, 2009, **54**, 2436.

33. M. M. Al Motari, M. E. Kandil, K. N. Marsh and A. R. H. Goodwin, *J. Chem. Eng. Data*, 2007, **52**.
34. F. J. P. Caetano, J. M. N. A. Fareleira, C. M. B. P. Oliveira and W. A. Wakeham, *J. Chem. Eng. Data*, 2005, **50**, 201.
35. X. Paredes, O. Fandiño, M. J. P. Comunas, A. S. Pensado and J. Fernandez, *J. Chem. Thermodyn.*, 2009, **41**, 1007.
36. K. R. Harris and S. Bair, *J. Chem. Eng. Data*, 2007, **52**, 272.
37. A. A. H. Padua, J. M. N. A. Fareleira, J. C. G. Calado and W. A. Wakeham, *J. Chem. Eng. Data*, 1996, **41**, 731.
38. X. Meng, P. Zheng, J. Wu and Z. Liu, *J. Chem. Eng. Data*, 2008, **53**, 1474.
39. F. Audonnet and A. A. H. Padua, *Fluid Phase Equil.*, 2004, **216**, 235.
40. A. S. Pensado, A. A. H. Padua, M. Comuñas and J. Fernandez, *J. Supercrit. Fluids*, 2008, **44**, 172.
41. E. Charles, J. Michel, P. Majbrunot, J. Molenat and H. Abachi, *J. Phys. E: Sci. Instrum.*, 1980, **13**, 829.
42. M. E. Kandil, K. N. Marsh and A. R. H. Goodwin, *J. Chem. Eng. Data*, 2007, **52**, 2382.
43. G. Dehestru, M. Leman, J. Jundt, P. Dryden, M. Sullivan and C. Harrison, *Rev. Sci. Instrum.*, 2011, **82**, 035113.
44. W. A. Wakeham, A. D. Fitt, K. A. Ronaldson and A. R. H. Goodwin, *High Temp. – High Pressures*, 2008, **37**, 137.
45. H. Faxen, *Ark. Matematik Astron. Fys.*, 1923, **17**, 1.
46. C. W. Oseen, *Ark. Matematik Astron. Fys.*, 1913, **9**, 1.
47. S. Goldstein, *Proc. Soc. Rheol.*, 1929, **123**, 225.
48. K. Fujii, Y. Fujita, N. Kuramoto and Y. Kurano, *24th JSTP*, 2003.
49. Y. Fujita, N. Kuramoto, Y. Kurano and K. Fujii, in *14th ICPWS*, 2004, p. 112.
50. T. Lommatzsch, M. Megharfi, E. Mahe and E. Devin, *Metrologia*, 2001, **38**, 531.
51. M. Brizard, M. Megharfi and C. Verdier, *Metrologia*, 2005, **42**, 298.
52. N. Mordant and J. F. Pinton, *Eur. Phys. J. B*, 2000, **18**, 343.
53. M. Brizard, M. Megharfi and E. Mahe, *Rev. Sci. Instrum.*, 2005, **76**, 025109.
54. Y. Kurano, H. Kobayashi, K. Yoshida and H. Imai, *Int. J. Thermophys.*, 1992, **13**, 643.
55. S. Feng, A. L. Graham, P. T. Reardon, J. Abbott and L. Mondy, *J. Fluids. Eng.*, 2006, **128**, 157.
56. P. Dauge, A. Baylaucq, L. Marlin and C. Boned, *J. Chem. Eng. Data*, 2001, **46**, 823.
57. S. Bair and F. Qureshi, *Tribol. Trans.*, 2002, **45**, 390.
58. A. Kumagai, D. Tomida and C. Yokoyama, *Int. J. Thermophys.*, 2006, **27**, 376.
59. D. I. Sagdeev, M. G. Fomina, G. K. Mukhamedzyanov and I. M. Abdulgatov, *J. Chem. Thermodyn.*, 2011, **43**, 1824.
60. G. J. Piermarini, R. A. Forman and S. Block, *Rev. Sci. Instrum.*, 1978, **49**, 1061.

61. R. G. Munro, S. Block and G. J. Piermarini, *J. Appl. Phys.*, 1979, **50**, 6779.
62. R. G. Munro, G. J. Piermarini and S. Block, *J. Appl. Phys.*, 1979, **50**, 3180.
63. A. Audetat and H. Keppler, *Science*, **303**, 513.
64. H. E. King Jr., E. Herbolzheimer and R. L. Cook, *J. Appl. Phys.*, 1992, **71**, 2071.
65. E. H. Abramson, *Phys. Rev. E*, 2007, **76**, 051203.
66. E. H. Abramson, *J. Chem. Phys.*, 2005, **122**, 084501.
67. J. J. Carty Jr., 1957, B.S. thesis, Massachusetts Institute of Technology, Cambridge, Massachusetts, USA.
68. E. H. Abramson and H. West-Foyle, *Phys. Rev. E*, 2008, **77**, 041202.
69. J. R. Smart, S. Beimfohr and D. T. Leighton Jr., *Phys. Fluids A*, 1993, **5**, 13.
70. K. P. Galvin, Y. Zhao and R. H. Davis, *Phys. Fluids*, 2001, **13**, 3108.
71. G. Meier, R. Vavrin, J. Kohlbrecher, J. Buitenhuis, M. P. Lettinga and M. Ratajczyk, *Meas. Sci. Technol.*, 2008, **19**, 034017.
72. E. H. Abramson, *Phys. Rev. E*, 2011, **84**, 062201.
73. R. L. Cook, H. E. King Jr., C. A. Herbst and D. R. Herschbach, *J. Chem. Phys.*, 1994, **100**, 5178.
74. K. U. Schug, H. E. King and R. Bohmer, *J. Chem. Phys.*, 1998, **109**, 1472.
75. R. L. Cook, C. A. Herbst and H. E. King Jr., *J. Phys. Chem.*, 1993, **97**, 2355.
76. B. Grocholski and R. Jeanloz, *J. Chem. Phys.*, 2005, **123**, 204503.
77. R. L. Cook, H. E. King Jr. and D. G. Peiffer, *Macromolecules*, 1992, **25**, 2928.
78. E. H. Abramson, *Phys. Rev. E*, 2009, **80**, 021201.
79. E. H. Abramson, *High Pressure Res.*, 2011, **31**, 544.
80. S. Klotz, K. Takemura, T. Strassle and T. Hansen, *J. Phys: Condens. Matter*, 2012, **24**, 325103.
81. S. Pawlus, S. Klotz and M. Paluch, *Phys. Rev. Lett.*, 2013, **110**, 173004.
82. M. Matsui, E. Ito, T. Katsura, D. Yamazaki, T. Yoshino, A. Yokoyama and K.-I. Funakoshi, *J. Appl. Phys.*, 2009, **105**, 013505.
83. E. F. May, M. R. Moldover and R. F. Berg, *Int. J. Thermophys.*, 2007, **28**, 1085.
84. E. F. May, M. R. Moldover, R. F. Berg and J. J. Hurly, *Metrologia*, 2006, **43**, 247.
85. J. T. Zhang, H. Lin and J. Che, *Metrologia*, 2013, **50**, 377.
86. R. F. Berg, E. F. May and M. R. Moldover, *J. Chem. Eng. Data*, 2014, **59**, 116.
87. M. R. Moldover, R. M. Gavioso, J. B. Mehl, L. Pitre, M. de Podesta and J. T. Zhang, *Metrologia*, 2014, **51**, R1.
88. L. Pitre, F. Sparasci, D. Truong, A. Guillou, L. Risegari and M. E. Himbert, *Int. J. Thermophys.*, 2011, **32**, 1825.
89. E. Vogel, B. Jäger, R. Hellmann and E. Bich, *Mol. Phys.*, 2010, **108**, 3335.
90. J. B. Mehl, unpublished calculations, 2013.
91. J. B. Mehl, M. L. Huber and A. H. Harvey, *Int. J. Thermophys.*, 2010, **31**, 740.
92. J. D. Wright, T. Cobu, R. F. Berg and M. R. Moldover, *Flow Meas. Instrum.*, 2012, **25**, 8.

93. R. F. Berg and M. R. Moldover, *J. Phys. Chem. Ref. Data*, 2012, **41**, 43104.
94. W. Cencek, M. Przybytek, J. Komasa, J. B. Mehl, B. Jeziorski and K. Szalewicz, *J. Chem. Phys.*, 2012, **136**, 224303.
95. R. F. Berg, *Metrologia*, 2005, **16**, 11. *Erratum*, 2006, **43**, 183.
96. R. S. Srivastava, *J. Appl. Math. Phys.*, 1980, **31**, 297.
97. M. Kawata, K. Kurase, A. Nagashima and K. Yoshida, in *Measurement of the Transport Properties of Fluids*, ed. W. A. Wakeham, A. Nagashima and J. V. Sengers, Blackwell Scientific Publications, Oxford, UK, 1991, pp. 49–76.
98. M. Rojas-Cardenas, I. Graur, P. Perrier and J. G. Meolans, *Phys. Fluids*, 2013, **25**, 072001.
99. S. Solomon, *Nature*, 2004, **427**, 289.
100. R. Krauss, J. Luettmer-Strathmann, J. V. Sengers and K. Stephan, *Int. J. Thermophys.*, 1993, **14**, 951.
101. D. Ripple and D. Defibaugh, *J. Chem. Eng. Data*, 1997, **42**, 360.
102. A. Laesecke, T. O. D. Lüddecke, R. F. Hafer and D. J. Morris, *Int. J. Thermophys.*, 1999, **20**, 401.
103. L. Schiller, *Drei Klassiker der Strömungslehre: Hagen, Poiseuille, Hagenbach*, Akademische Verlagsgesellschaft, Leipzig, 1933.
104. D. A. Edwards and C. F. Bonilla, *Ind. Eng. Chem.*, 1944, **36**, 1038.
105. W. H. Mears, R. F. Stahl, S. R. Orfeo, R. C. Shair, L. F. Kells, W. Thompson and H. McCann, *Ind. Eng. Chem.*, 1955, **47**, 1449.
106. T. W. Phillips and K. P. Murphy, *J. Chem. Eng. Data*, 1970, **15**, 304.
107. T. W. Phillips and K. P. Murphy, *ASHRAE Trans.*, 1970, 77(Part II), 146.
108. I. R. Shankland, in *AIChE Spring National Meeting, Symposium on Global Climate Change and Refrigerant Properties*, Orlando, FL, 1990, p. 31.
109. I. R. Shankland, R. S. Basu and D. P. Wilson, in *Meeting of IIR Commissions B1, B2, E1, E2*, West Lafayette, IN, 1988, pp. 305–314.
110. E. H. Eisele, W. E. Fontaine and W. Leidenfrost, in *12th Int. Congr. Refrig. Prog. Refrig. Sci. Technol.*, 1969.
111. D. T. Gordon, J. F. Hamilton and W. E. Fontaine, *ASHRAE Trans.*, 1969, **75**, 40.
112. M. R. Cannon, R. E. Manning and J. D. Bell, *Anal. Chem.*, 1960, **32**, 355.
113. A. Kumagai and S. Takahashi, *Int. J. Thermophys.*, 1991, **12**, 105.
114. L.-Z. Han, M.-S. Zhu, X.-Y. Li and D. Luo, *J. Chem. Eng. Data*, 1995, **40**, 650.
115. L.-Q. Sun, M.-S. Zhu, L.-Z. Han and Z.-Z. Lin, *J. Chem. Eng. Data*, 1996, **41**, 292.
116. D. Ripple, *Rev. Sci. Instrum.*, 1992, **63**, 3153.
117. D. Ripple and O. Matar, *J. Chem. Eng. Data*, 1993, **38**, 560.
118. D. S. Cousins and A. Laesecke, *J. Res. Natl. Inst. Stand. Technol.*, 2012, **117**, 231.
119. A. Kumagai and C. Yokoyama, *Int. J. Thermophys.*, 2000, **21**, 909.
120. G. D. Wedlake, J. H. Vera and G. A. Ratcliff, *Rev. Sci. Instrum.*, 1979, **50**, 93.
121. A. Laesecke and R. F. Hafer, *J. Chem. Eng. Data*, 1998, **43**, 84.

122. Y.-Y. Duan, L. L. Shi, L.-Z. Han and M.-S. Zhu, *Fluid Phase Equilib.*, 1999, **162**, 303.
123. X.-J. Liu, L. L. Shi, L.-Z. Han and M.-S. Zhu, *J. Chem. Eng. Data*, 1999, **44**, 688.
124. J. Wu, Z. Liu, S. Bi and X. Meng, *J. Chem. Eng. Data*, 2003, **48**, 426.
125. I. M. Sivebaek, S. C. Sorenson and J. Jakobsen, 2001, SAE Technical Report.
126. A. Laesecke, R. F. Hafer and D. J. Morris, *J. Chem. Eng. Data*, 2001, **46**, 433.
127. R. A. Dawe, Ph.D. thesis, University of Oxford, 1968.
128. R. A. Dawe, *Rev. Sci. Instrum.*, 1973, **44**, 1231.
129. S. A. Berger, L. Talbot and L.-S. Yao, *Annu. Rev. Fluid Mech.*, 1983, **15**, 461.
130. M. L. Huber, A. Laesecke and R. A. Perkins, *Ind. Eng. Chem. Res.*, 2003, **42**, 3163.